Conformal high-entropy oxide coatings enable fast and durable surface oxygen reactions

F. He, K. Sasaki

To be published in "Joule"

June 2025

Chemistry Department

Brookhaven National Laboratory

U.S. Department of Energy

USDOE Office of Energy Efficiency and Renewable Energy (EERE), Office of Sustainable Transportation. Hydrogen Fuel Cell Technologies Office (HFTO)

DISCLAIMER

Conformal High-entropy Oxide Coatings Enable Fast and Durable Surface Oxygen Reactions

Fan He[1], Hao Liu[1], Yangsen Xu[1], Feng Zhu[1], Kotaro Sasaki[2], YongMan Choi[3]**, Ying Liu[4]***, and Yu Chen[1]*

[1]School of Environment and Energy, South China University of Technology, 382 East Road, Higher Education Mega Center, Guangzhou 510006, P. R. China.
[2]Chemistry Division, Brookhaven National Laboratory, Upton, NY 11973, USA
[3]College of Photonics, National Yang Ming Chiao Tung University, Tainan 71150, Taiwan
[4]Research Institute of Renewable Energy and Advanced Materials, Zijin Mining Group Co., Ltd., Xiamen, Fujian 361101, China
*Correspondence: eschenyu@scut.edu.cn
**Correspondence: ymchoi@nycu.edu.tw
**Correspondence: liu_ying@zijinmining.com

SUMMARY

Developing active and durable air electrodes for efficient oxygen reactions is challenging for protonic ceramic cells (PCCs), especially at temperatures below 550 °C, due to the sluggish oxygen reaction kinetics and insufficient structural stability in high humidity conditions. Here, we report a rational-designed conformal coating with a high-entropy $PrNi_{0.2}Mn_{0.2}Co_{0.2}Fe_{0.2}Cu_{0.2}O_{3-\delta}$ (PNMCFC) perovskite structure on the surface of a state-of-the-art $PrBaCo_2O_{5+\delta}$ (PBC) air electrode. The formed hybrid air electrode (PNMCFC-PBC) shows faster surface oxygen kinetics and a more stable phase structure in high-humidity air than the bare PBC electrode, as demonstrated by the electrical conductivity relaxations and surface composition analyses. Further density functional theory (DFT) calculations suggest that the conformal coating can mitigate Ba segregation at the interface and improve oxygen-related reactions, enhancing overall stability and electrocatalytic performance. The cells with the developed hybrid electrodes show encouraging electrochemical performance at 550 °C: a polarization resistance of 0.72 Ω cm^2, a peak power density of 1.30 W cm^{-2}, an electrolysis current density of -1.36 A cm^{-2} at 1.3 V, and reasonable operating stabilities (~200 h at 550 °C). Our progress in this study offers valuable guidance for the design of next-generation PCC air electrodes.

KEYWORDS

Protonic ceramic cells; High-entropy materials; Air electrodes; Activity; Conformal coating.

INTRODUCTION

Energy conversion and storage technologies continuously innovate to establish a sustainable system with a cheaper and more efficient energy supply.[1-4] Among all types of technologies, reversible protonic ceramic cells (PCCs) are one of the most efficient devices with excellent fuel flexibility, versatile functionality, and emission-free power generation.[5-9] However, their inclusion in competitive commercialization requires further maturation on the operating temperature, cost, and lifetime.[10-12] Reduction in operating temperatures often causes a dramatic increase in electrochemical resistance of cell components, especially of air electrodes, due to the sluggish activation of oxygen exchange kinetics at low temperatures.[13-15] More commercially viable attention has been drawn to electrodes with superior durability against high-concentration steam and high activity for the oxygen reduction and evolution reactions (ORR and OER) under realistic operating conditions of PCCs.

Managing the impact of humidity on the phase structure and catalytic activity became a key technical direction for improving the durability and electrochemical performance of electrodes in PCCs.[16-18] Many state-of-the-art electrodes, such as $La_{0.6}Sr_{0.4}Co_{0.2}Fe_{0.8}O_{3-\delta}$ (LSCF),[19] $Ba_{0.5}Sr_{0.5}Co_{0.8}Fe_{0.2}O_{3-\delta}$ (BSCF),[20] $PrBaCo_2O_{5+\delta}$ (PBC),[21] and $PrBa_{0.5}Sr_{0.5}Co_2O_{5+\delta}$ (PBSC),[22] have demonstrated excellent mixed conductivity and fast ORR/OER kinetics whereas displayed dramatic performance degradations under the operating conditions of PCCs (500-600 °C and high steam concentration). A steam-containing environment is commonly encountered during the operation of PCCs, while steam-mediated phase segregations have been recently reported near the surface of most Sr(Ba)-based perovskite oxides or electrode-electrolyte interface.[23,24] One modification strategy is essential for structural improvement against negative water-mediated segregation. Sr (Ba)-free electrodes have been investigated as the first candidate for enhanced stability in PCC, such as La(Ni, Fe)$O_{3-\delta}$, nano-fiber Pr_2NiO_4, and $Ca_3Co_4O_{9-\delta}$.[25,26] The high- or medium-entropy concept has been introduced to develop new electrode materials and architectures with good resistance to steam.[27,28] Although the chemical system of those compounds becomes more and more complicated,[29] the durability of the high-entropy air electrode has been largely improved under realistic cell conditions with high concentrations of steam.[22,30] A more facile and economical method for surface modification is wet-chemical solution infiltration, which has been extensively utilized in electrocatalysis, photocatalysis, membrane reactors, and fuel cells.[31-33]

Most solution infiltrations are to decorate abundant highly active catalysts on the surface of the substrates. However, the discrete nano-catalysts may play an unsatisfactory role in the structural stability against surface segregation since the steam penetrates the pores within the surface layer.[34] The driving forces to element segregation may originate from the electrostatic interaction between A-site cations with negative charges and surface oxygen vacancies with positive charges, which is mainly associated with the surface adsorbates.[24] A few studies demonstrated that dense $La_{0.85}Sr_{0.15}MnO_{3-\delta}$ (LSM) conformally coated porous LSCF catalyst can effectively suppress Sr segregation for an enhanced stability of solid oxide fuel cells (SOFCs).[1,35] The porous LSCF backbone functions as a channel for the fast transport of oxygen ions and electrons, while dense thin-film LSM coating diminishes the surface electrostatic force of LSCF for enhanced durability.[35] However, the air electrodes in PCCs face higher concentrations of steam in the air (up to 30 vol%).[6] Maintaining the structural stability of PCC air electrodes is much more difficult than the traditional cathode for oxygen-ion conducting solid oxide fuel cells (O-SOFCs). Thus, one pivotal strategy is to develop a desired coating that should possess a conformal coverage of the backbone, excellent activities for ORR and OER, and high structural tolerance to steam and even to carbon dioxide encountered in reversible PCC operation.

Inspired by the aforementioned methods and requirements, we showcase a Ba(Sr)-free high-entropy conformal perovskite coating, $PrNi_{0.2}Mn_{0.2}Co_{0.2}Fe_{0.2}Cu_{0.2}O_{3-\delta}$ (PNMCFC), successfully covered onto the PBC backbone for enhanced electrocatalytic activity and durability of PCCs. The selection of B-site cations close to Co ions in the PNMCFC perovskite may lead to the fast oxygen exchange kinetics and versatile functionalities as a so-called "Cocktail" effect,[36] as determined by electrical conductivity relaxations (ECR) results and low polarization resistances (R_p). According to the equation of $\Delta G_{mix} = \Delta H_{mix} - T\Delta S_{mix}$, the structural stability of high-entropy PNMCFC ($\Delta S_{mix} > 1.5R$, R is gas constant) is largely enhanced compared to the PBC electrode.[37] Additionally, density functional theory (DFT) calculations were applied to support the experimental findings by investigating the enhanced electronic interactions, efficient surface oxygen kinetics, and migration of Ba cations facilitated by the conformal coating on the PBC backbone using the high-entropy PNMCFC. When compared with the PBC electrode, the conformal PNMCFC-coated PBC electrode (hybrid electrode) performs lower area-specific resistance and higher electrochemical performances in fuel-cell mode (2.29 W cm^{-2} at 650 °C) and electrolysis mode (-3.12 A cm^{-2} at 1.3V and 650 °C) modes. Our high-entropy conformal coating strategy could optimize the mixed ion-conducting air electrode materials to realize structural stability against high-concentration steam encountered in realistic PCC operation. Not limited to fuel-cell stability in ambient air, the cells with the hybrid electrode also exhibit excellent stabilities in electrolysis and reversible cycling under conditions of highly humidified air (30% H_2O) and large current density (-1A cm^{-2}).

RESULTS AND DISCUSSION

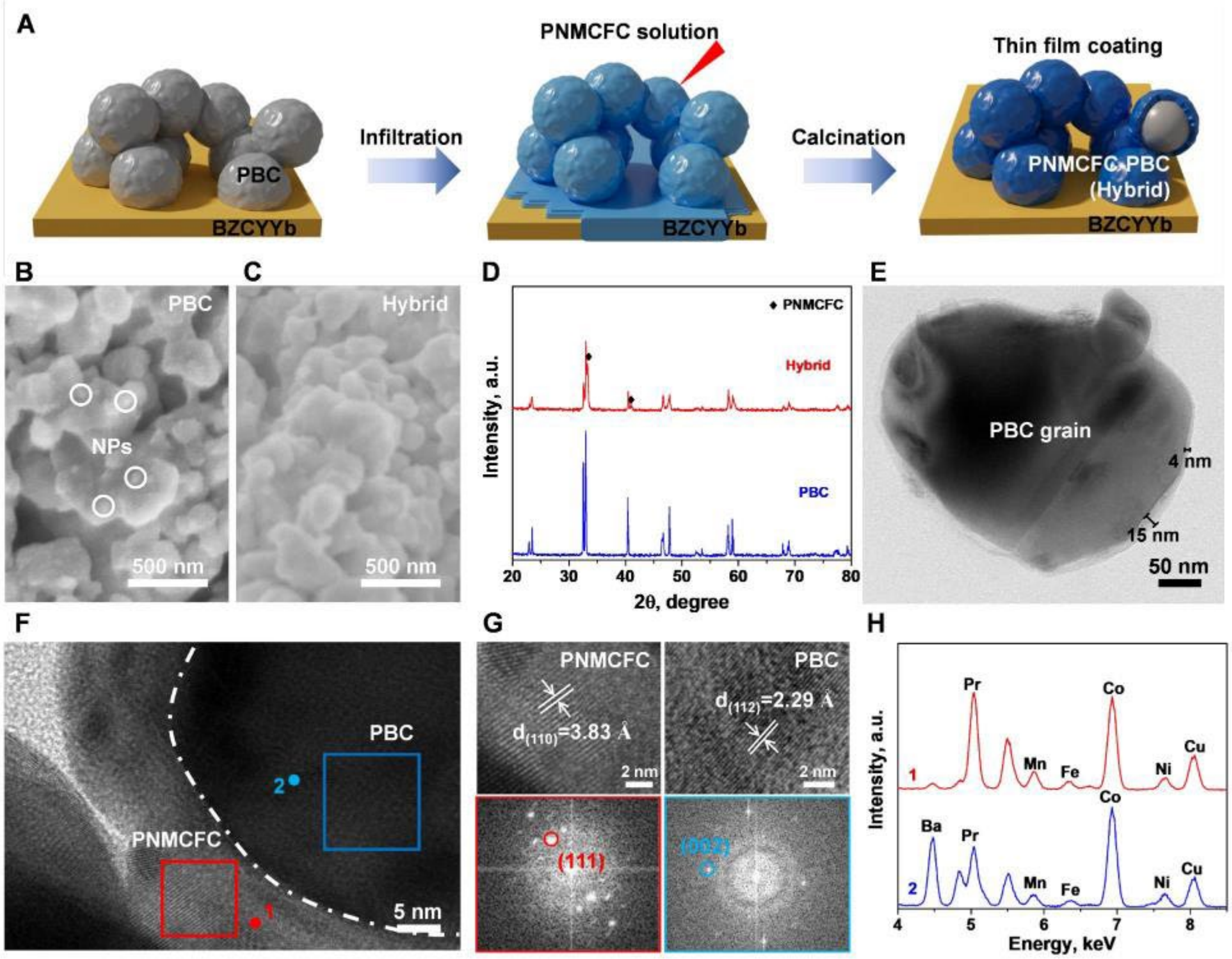

Figure 1. Morphology and crystal structure of the hybrid electrode.
(A) Schematic of a PBC electrode backbone covered with a conformal high-entropy PNMCFC coating.
(B and C) (B) SEM images of the PBC and (C) PNMCFC-coated PBC hybrid electrodes.
(D) XRD patterns of the PBC and PNMCFC-coated PBC hybrids.
(E) STEM image of a whole PBC grain covered by a conformal PNMCFC coating.
(F) A high resolution-TEM image of the PBC grains covered with a conformal PNMCFC coating.
(G) Enlarged TEM images of PNMCFC coating and PBC backbone (top); the bottoms are the FFT patterns from the red and blue rectangles in (F).
(H) EDS spectra from points 1 and 2, indicating that the outer surface is mainly PNMCFC (point 1) while the inside is PBC and PNMCFC hybrid grains (point 2).

Structural characterization of high-entropy conformal perovskite coating

Ba (Sr)-free high-entropy perovskite, $PrNi_{0.2}Mn_{0.2}Co_{0.2}Fe_{0.2}Cu_{0.2}O_{3-\delta}$ (PNMCFC), displayed an orthorhombic structure with the space group of *Pnma* and lattice parameters of a=5.4340 Å, b=7.6744 Å, and c=5.4506 Å (χ^2=0.47, **Figure S1** and **Table S1**). The actual atomic ratio of each element in as-synthesized PNMCFC was examined by inductively coupled plasma-mass spectrometry (ICP-MS), which closely approaches the nominal chemical stoichiometric ratio (**Table S2**). When employed to cover the whole surface of a porous PBC electrode, differing from the modifications with nanoparticles, the conformal thin-film PNMCFC coating enables complete isolation of the PBC backbone from steam exposure during harsh PCC operational conditions, thereby probably enhancing system durability. The structural similarity of PNMCFC to PBC facilitates the conformal growth of a dense and well-connected coating during high-temperature thermal calcination (**Table S1**). **Figure 1A** schematically exhibits the whole process of the thin-

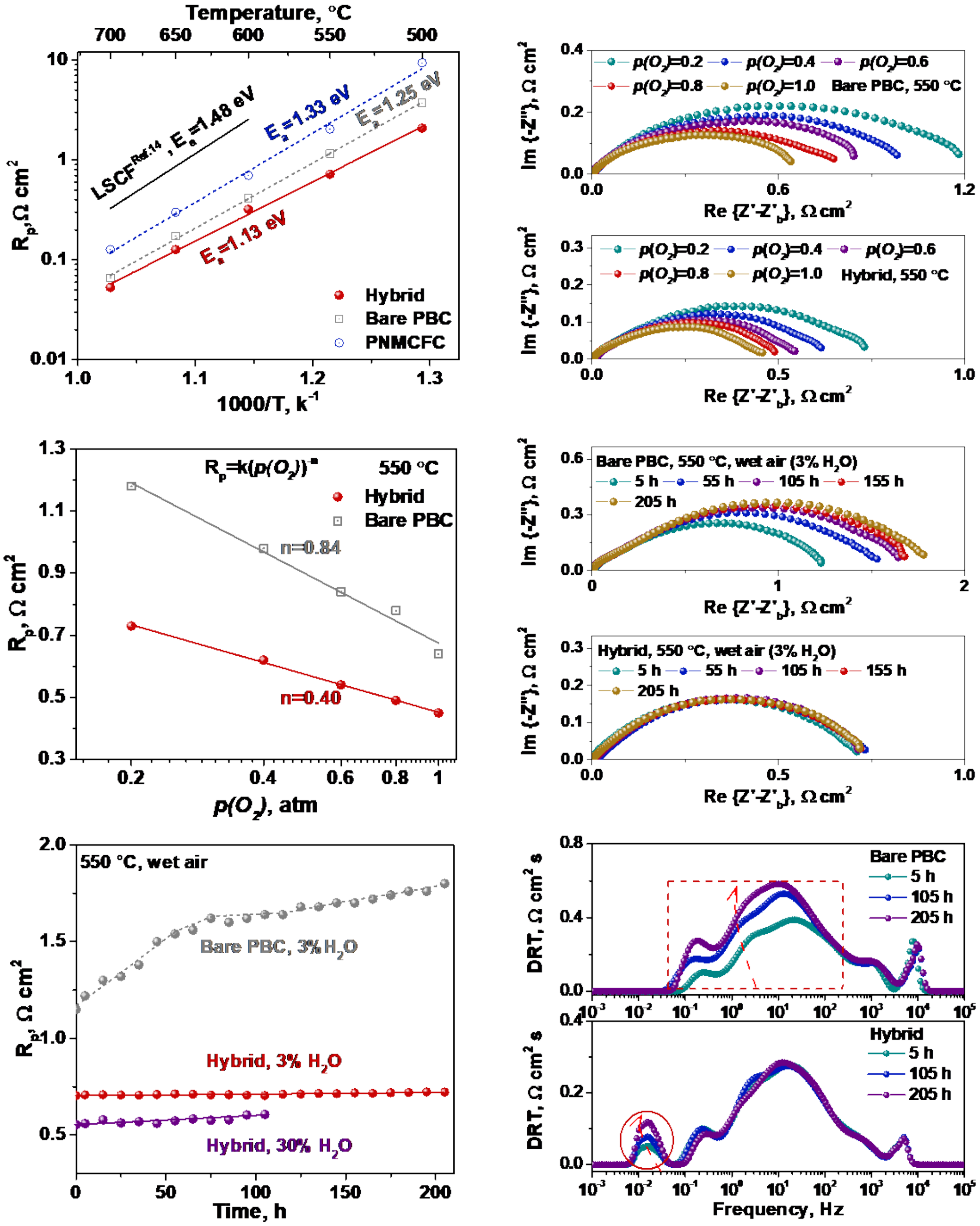

Figure 2. Electrochemical performance and durability of the hybrid electrodes.

(A) Arrhenius plots of the polarization resistance of bare PBC, PNMCFC and hybrid (PNMCFC-PBC) electrodes.

(B) EIS of bare PBC and hybrid electrodes as a function of $p(O_2)$ at 550 °C.

(C) Dependence of each R_p of bare PBC and hybrid electrodes as a function of $p(O_2)$ at 550 °C.

(D) EIS of bare PBC (top) and hybrid electrodes (bottom) at different testing times in wet air (3% H_2O) and 550 °C.

(E) Time dependence of R_p of bare PBC and hybrid electrodes in wet air (3% and 30% H_2O) at 550 °C.

(F) DRT analysis of bare PBC (top) and hybrid electrodes (bottom) at different testing times according to the EIS data in (d).

film formation of a high-entropy catalyst coating onto a PBC backbone. Many nanoparticles (NPs) were covered on the surface of the PBC electrode, which was likely associated with the $BaCoO_{3-\delta}$ phase (**Figure 1B**). While the hybrid (PNMCFC-PBC) electrode maintained a relatively smooth surface with a larger average grain size of 550 nm (**Figure 1C** and **S2**). According to the X-ray diffraction (XRD) patterns (**Figure 1D** and **Figure S3**), the PNMCFC phase was successfully observed on the hybrid electrode. Briefly, 3 μL of 0.1 M PNMCFC nitrate organic solution was infiltrated into the PBC backbone (loading of ~0.3 mg cm^{-2}), followed by thermal calcination at 950 °C for 5 h to form the PNMCFC coating PBC hybrid electrode. **Figure 1E** demonstrated that the PBC surface was coated by a conformal and continuous PNMCFC thin film with a projected thickness of 4-15 nm. The high-temperature calcination and structural similarity led to the coherent coating, which can be commonly observed (**Figure S4**). As obtained by high-resolution transmission electron microscopy (HR-TEM), the space distances of 3.83 and 2.29 Å were assigned to the (110) plane of PNMCFC and (112) plane of PBC, respectively (**Figure 1F and 1G**, top). The two different phases of surface coating and bulk grain were well distinguished via the fast Fourier transform (FFT) on the red and blue rectangles in **Figure 1F**. The marked diffraction spots corresponded to the (111) plane of PNMCFC and the (002) plane of PBC, which was consistent with the XRD refinement (**Figure 1G**, bottom). The X-ray energy dispersive spectrum (EDS) spectra (**Figure 1H**) indicated that the surface coating is mainly PNMCFC (point 1), while the bulk substrate is composed of PNMCFC and PBC hybrid phases (point 2). The slight cation thermal diffusion also occurred between PNMCFC and PBC after thermal calcination at 950 °C for 5 h, as checked by the peak belonging to Ba at point 1. The discrepancy in the elemental composition with the line scanning from bulk to surface further supported the formation of the unique architecture of PNMCFC thin-film coated PBC (**Figure S5**).

Electrochemical performance and durability

Shown in **Figure 2A** are the Arrhenius plots of the polarization resistance (R_p) of the BZCYYb-supported symmetrical cells with the bare PBC, PNMCFC and hybrid electrodes, combined with the comparison of the typical commercial LSCF electrode as reported.[16] The hybrid electrode achieved a lower R_p (0.72 Ω cm^2 at 550 °C) and activated energy (E_a, 1.13 eV) than the PBC (1.16 Ω cm^2 at 550 °C, 1.25 eV) and PNMCFC electrode (2.04 Ω cm^2 at 550 °C, 1.33 eV), much better than the LSCF electrode recently reported (**Figure S6**).[16] The R_p of the hybrid electrodes showed no apparent decrease when the concentration of infiltration solution increased from 0.1 to 0.2 M, leading to the solution concentration fixed at 0.1 M (**Figure S7**). The influence of the PNMCFC coating on PBC electrode surface reaction kinetics was further investigated via the electrochemical resistances measured under different oxygen partial pressures ($p(O_2)$) (**Figure 2B**). The specific rate-limiting step for surface oxygen exchange kinetics can be fitted by R_p dependence on $p(O_2)$, which is expressed as the equation of $R_p = k(p(O_2))^{-n}$ (n is reaction order, k is constant).[38] Clearly, note that the n value of the hybrid electrode is largely changed from the original 0.84 of the PBC electrode to 0.40 (**Figure 2C**). n=0.84 of the PBC electrode may be related to the gas diffusion on the electrode surface.[39,40] When n=0.375, the first charge transfer reaction of ($O_{ads} + e^- + V_{O(s)}^{\bullet\bullet} \leftrightarrow O_{O(s)}^{\bullet}$) is a key rate-limiting step for hybrid electrodes.[39,40] This result indicates that the ORR process of PNMCFC-PBC is mainly controlled by the surface oxygen vacancy concentration,[41] differing from that of the PBC electrode (which is controlled by the mass transfer). To verify this, we analyzed O 1s X-ray photoelectron spectroscopy (XPS) spectra of PBC, PNMCFFC, and PNMCFC-PBC (**Figure S8**). It was found that the $O_{ad}/O_{lattice}$ ratio of the PNMCFC-PBC was reduced to 2.08 compared to the PBC (its $O_{ad}/O_{lattice}$ ratio is 2.43), suggesting the surface oxygen vacancy concentration of the hybrid sample decreased. The electrical conductivities of the PNMCFC and PNMCFC-PBC reached 1.5-4.8 S cm^{-1} and 564-1175 S cm^{-1} at 400-750 °C, respectively, which were lower than those (620-1215 S cm^{-1} at 400-750 °C) of the PBC (**Figure S9**). Thus, the surface vacancy concentration and electrical conductivities of the PNMCFC coating may lead to changes in hybrid electrode kinetics from surface gas diffusion (rate-limiting step of PBC) to the charge transfer reaction.

Numerous highly active air electrodes are closely associated with $Sr(Ba)CoO_3$-based perovskite oxides,[23] while their stability under humidified air is poor due to phase segregation, especially in reversible

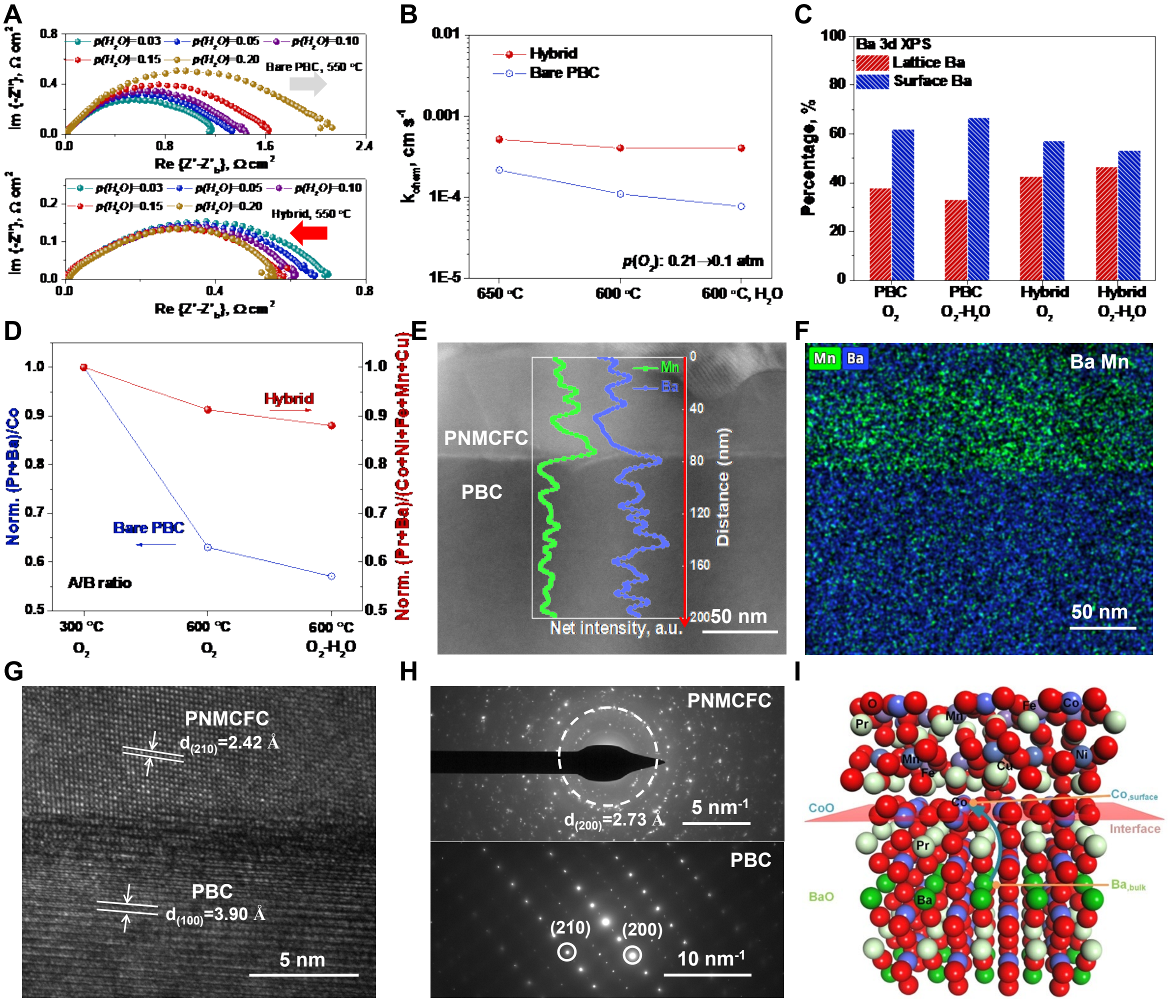

Figure 3. Investigation on the enhanced durability of the hybrid electrode.

(A) EIS of bare PBC and hybrid PNMCFC-PBC as a function of $p(H_2O)$ at 550 °C.

(B) k_{chem} of bare PBC and PNMCFC-PBC measured at 650 °C, and 600 °C before and after a treatment in wet air (10% H_2O) for 100 h.

(C) Surface Ba composition of PBC and hybrid catalyst at 600 °C measured under different conditions: pure O_2 at 600 °C, and humidified gas mixture (10% H_2O-90% O_2) at 600 °C.

(D) (Pr+Ba)/Co ratio of PBC and (Pr+Ba)/(Co+Ni+Fe+Mn+Cu) ratio of hybrid catalyst when measured under different conditions: pure O_2 at 300 °C, pure O_2 at 600 °C, and humidified gas mixture (10% H_2O-90% O_2) at 600 °C; the ratio of A-site and B-site cations was normalized by that obtained in O_2 at 300 °C.

(E) Cross-sectional TEM micrograph of a conformal PNMCFC-deposited PBC substrate; inset is EDS linear profile across the PNMCFC coating to PBC substrate along the red arrow.

(F) EDS mapping of Ba and Mn element distributions.

(G and H) (G) HR-TEM and (H) SAED images of PNMCFC coating (top) and PBC substrate (bottom).

(I) Schematic illustration of Ba cation segregation from the bulk to the surface of PBC(001) following the conformal coating of PNMCFC. The segregation energy of the Ba cation is calculated to be 2.36 eV for the PNMCFC-coated PBC(001), compared to 0.48 eV for bare PBC(001).

PCCs. As shown in **Figures 2D** and **2E**, the PBC electrode demonstrated a dramatic R_p deterioration rate of 0.317 Ω cm^2 per 100 h at 550 °C in wet air (3% H_2O). The high-entropy PNMCFC coating efficiently enhances structural tolerance against steam, as indicated by an R_p deterioration rate of only 0.008 Ω cm^2 per 100 h for comparison. Even in the air with higher humidity (30% H_2O), the R_p of the PNMCFC-PBC hybrid electrode can remain relatively stable, which slightly increased from 0.553 to 0.607 Ω cm^2. The surface electrode kinetics evolutions can be ascertained by the distribution of relaxation time (DRT) analysis on the EIS spectra at different times. Each DRT curve seems to have at least three processes for the electrode reactions, which correspond to low frequency (LF, ≤10^0 Hz, mass transfer near the interface), intermediate frequency (IF, 10^0-10^3 Hz, surface exchange processes), and high frequency (HF, ≥10^3 Hz, charge transfer), respectively.[38] The lasting increases in R_p of the PBC electrode were concentrated in the intermediate frequency range of 10^2-10^{-1} Hz, while the extra low-frequency peaks at 10^{-1}-10^{-2} Hz appeared on the DRT curves of the hybrid electrode, which included the main R_p variations (**Figure 2F** and **Figure S10**). Compared to the DRT curves of the PBC electrode, the extra low-frequency peaks at 10^{-1}-10^{-2} Hz are likely associated with the surface electrode reaction of PNMCFC coating.[38] Thus, the PNMCFC coating may alter the mass transfer process on the electrode surface while ensuring that the PBC backbone maintains structural integrity and fast bulk ion transfer.

Origin of the durability improvement

Changing steam partial pressure (*$p(H_2O)$*) from 3 to 20 vol% makes a dramatic decrease in the R_p of the hybrid electrode from 0.69 to 0.54 Ω cm^2 (**Figure 3A**, bottom). The electrochemical reactions of the hybrid electrode can be deconvoluted by DRT analysis on the EIS in the air containing different *$p(H_2O)$* (**Figure S11**). As fitted by the equation of $R_p = k(pH_2O)^{-m}$, the reaction order of m value can determine the rate-limiting step of isolated electrode reaction at each frequency range. The R_p of peaks at the low-frequency range (reaction order m of 0.83) are more sensitive to *$p(H_2O)$*. Note that m=1, $H^+_{TPB} + OH^-_{TPB} \rightarrow H_2O_{TPB}$ and $H_2O_{TPB} \rightarrow H_2O_{(g)}$ are highly associated with the key rate-limiting steps.[42] These results indicate that the electrochemical reactions of the PNMCFC-PBC in wet air are likely controlled by mass transfer and gas diffusion on the electrode surface. In addition, the impedances of the peaks at intermediate and low frequencies were dramatically reduced, corresponding to the ionic diffusion and mass transfer process, respectively. This result suggests that PNMCFC coating can optimize the PBC electrode electrochemical processes of ionic diffusion and mass transfer. The behavior of the bare PBC electrode is distinctive from that of the hybrid electrode, which performed a sharp increase from 1.15 to 2.13 Ω cm^2 under identical conditions (**Figure 3A**, top). Water-induced phase segregation may occur at the surface of the PBC electrode, impacting the surface exchange kinetics of oxygen reactions. To prove this hypothesis, the surface exchange coefficients (k_{chem}) of the PBC and PNMCFC-PBC were further investigated by ECR (**Figure S12** and **3B**). The hybrid electrode exhibits higher k_{chem} than the PBC electrode at 500-650 °C, resulting in better electrochemical performance (**Figure S12**). A more obvious decrease of k_{chem} at 600 °C was obtained on the PBC electrode compared to the hybrid electrode after the interaction with the steam (10% H_2O) for 100 h (**Figure 3B** and **S13**). The corresponding surface chemistry of the PBC and hybrid samples was investigated via X-ray photoelectron spectroscopy (XPS), quantified from Ba $3d_{5/2}$, Co $2p_{3/2}$, and O 1s spectra (**Figure 3C**, **S14**, and **S15**). Compared to the PBC sample measured in O_2 at 600 °C, the surface Ba contents were induced for segregation from 62% to 66% with the steam (10% H_2O) injecting (**Figure 3C** and **S14A**). Differing from PBC, the PNMCFC-PBC performed a contrary tendency from 57% to 54% after the identical steam pretreatments (**Figure 3C** and **S14B**), indicating that the Ba segregation of PBC was suppressed by the PNMCFC thin-film coating. Combined with the O1s results, a large amount of Ba segregation at the PBC surface caused vacancy formation for the increased adsorbed oxygen (O_{ad}) (**Figure S15**). The phase structure of the PNMCFC-PBC remains stable before and after the treatment of humidified oxygen, as checked from the Ba 3d and O1s XPS (**Figure 3C** and **S15**). To more visually reveal how the PNMCFC coating inhibits the element segregation, we provided the surface atomic information of PBC and hybrid samples by XPS analyses under different measured conditions of O_2 at 300 °C, O_2 at 600 °C, and 10% H_2O-90% O_2 at 600 °C, which are expressed as the ratio of A-site and B-site cations (**Figure 3D** and **Table S3**). The samples were firstly decarbonized for normalization in pure O_2 at 300 °C, then heated to 600 °C, and finally exposed to the humidified O_2 (10% H_2O). The (Pr+Ba)/Co ratio of PBC dramatically decreased in such an operating process due to the severe Ba segregation under oxygen/steam-rich conditions. In contrast, the surface of the PNMCFC-PBC performed a relatively balanceable A/B-site ratio, efficiently enhancing the structural stability of the PBC substrate.

To obtain the mechanism for excellent steam-tolerance durability of hybrid electrodes, a more detailed morphology of the lattice maintenance and robust interface growth between PBC and PNMCFC was examined by the focused ion beam (FIB)-TEM. PNMCFC was firstly deposited onto the surface of the dense PBC substrate and then thermally calcined at 950 °C for 5 h. Shown in **Figure 3E** is the cross-sectional TEM image of the PNMCFC deposited PBC dense substrate after the steam (10% H_2O) pretreatments at 600 °C. Fewer elements can be utilized for phase differentiation due to the high similarity between PNMCFC and PBC phases and cation thermal diffusion during calcination, and the representative Ba and Mn elements were chosen for linear scanning and mapping. The content of Mn and Ba at the interface is likely caused by the cation thermal diffusion during high-temperature calcination at 950 °C for 5 h. EDS linear profiles and mapping (**Figure 3E (inset), 3F, and S16)** demonstrated that the PNMCFC thin film was conformally coated on the PBC substrate with enhanced durability against steam. According to the element contents from the EDS results (**Figure S17**), the PBC maintains full structural integrity by protecting the conformal PNMCFC coating against a steam-containing environment. As clearly observed by HR-TEM (**Figure 3G**), the PNMCFC phase epitaxially grew and kept well-connected with the PBC substrate to form a robust heterointerface. In addition, the PNMCFC layer maintains crystalline after interacting with steam, of which a space distance of 2.24 Å corresponds to the (211) plane, while the different space distance of 3.90 Å belongs to the (100) plane of the PBC lattice. The marked ring (top) and spots (bottom) from the selected area electron diffraction (SAED) can confirm that they can be assigned to the (200) plane of PNMCFC, (210), and (200) planes of PBC, respectively (**Figure 3h**).

DFT calculations were performed to investigate the conformal coating of high-entropy PNMCFC on PBC, demonstrating its effectiveness in enhancing PCC performance and stability by mitigating Ba segregation (**Note S1**). As summarized in **Figure S18** and **Table S4**, initial screening calculations were conducted to optimize the most plausible high-entropy bulk PNMCFC structure, yielding the most oxygen vacancy formation energy (E_{vac}) at 2.04 eV. The bulk lattice parameter of PNMCFC was adjusted to match PBC, assuming an ideal conformal coating. The recalculated E_{vac} values of 2.04 eV and 1.83 eV, respectively, showed a 10% reduction, indicating improved bulk properties. Following the surface stability analysis of PBC and PNMCFC surfaces (**Table S5** and **Figure S19**), the most stable surfaces were selected for segregation energy and O *2p*-band center calculations. As summarized in **Table S6**, the total O *2p*-band center for the hybrid PNMCFC/PBC(001) shifts closer to the Fermi energy (−2.51 eV) compared to the PNMCFC(001) surface (−3.04 eV). For the coated PNMCFC, the O *2p*-band center is calculated to be −2.57 eV, highlighting the enhanced electronic interaction and more efficient surface oxygen kinetics.[37] The shift indicates increased covalency of oxygen bonding at the interface, enhancing orbital overlap, charge transfer, and oxygen-related surface reactions.[43] Besides elucidating surface oxygen kinetics by understanding the O *2p*-band center, we conducted the segregation energy calculations of Ba cations from PBC to investigate the improved stability test results. As summarized in **Figures 3I**, **S19** and **Table S6**, the segregation energy of Ba increases significantly from 0.48 eV (bare PBC) to 2.36 eV (PNMCFC/PBC), verifying that Ba migration to the surface is energetically prohibitive after coating. In summary, the PNMCFC coating suppresses Ba migration by increasing segregation energy, strengthening oxygen bonding interactions, and acting as a physical barrier, resulting in improved structural stability of air electrodes. The state-of-the-art conformal coating approach offers valuable guidance for the rational design of next-generation high-entropy perovskite materials, paving the way for advancements in PCCs.

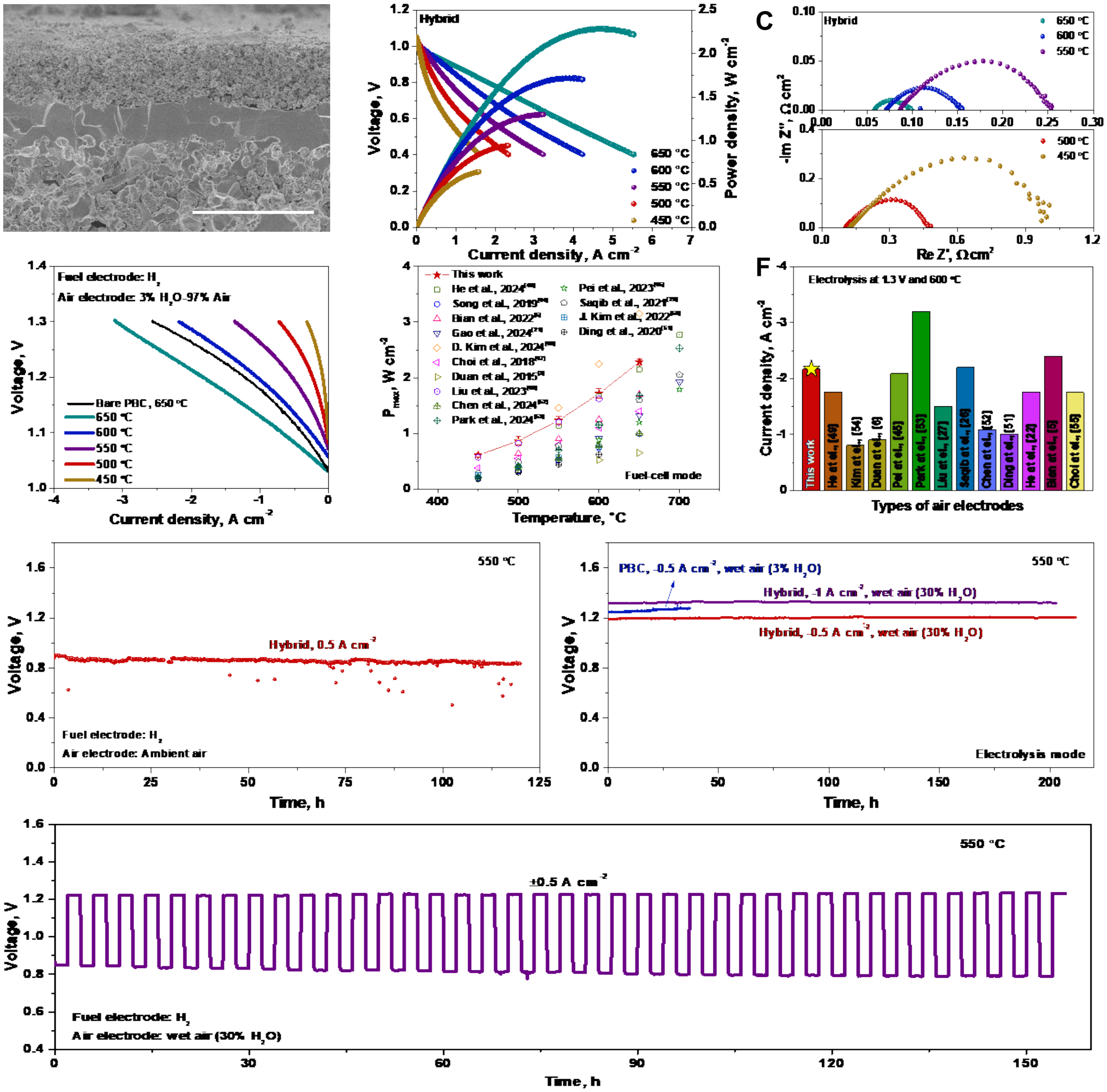

Figure 4. Electrochemical performance and durability of the single cells with the hybrid electrode.

(A) Cross-sectional SEM image of a fuel-electrode-supported single cell with the hybrid (PNMCFC-PBC) electrode.

(B and C) (B) Typical I-V-P curves and (C) EIS of single cells with the hybrid electrode at 450-650 °C.

(D) Typical I-V curves of single cells with the bare PBC (black line) at 650 °C and hybrid electrodes at 450-650 °C.

(E and F) (E) Comparisons of fuel cell P_{max} (**Table S7**) and (F) current densities at 1.3 V and 600 °C (**Table S8**).

(G) Stability of the single cells at 550 °C applied a current density of 0.5 A cm^{-2} (in fuel cell mode).

(H) current densities of -0.5 and -1.0 A cm^{-2} (in electrolysis mode); (i) Reversible cycling operation at current densities of ±0.5 A cm^{-2} at 550 °C.

Single-cell performance and durability

Shown in **Figure 4A** is the cross-sectional image of the single cell with the construction of Ni-BZCYYb fuel electrode, BZCYYb electrolyte (~ 6 μm), and hybrid (PNMCFC-PBC) air electrode. The I-V-P curves were recorded by fueling H_2 to the fuel electrode and exposing the air electrode to ambient air. The PBC electrode achieved a peak power density of 1.82 W cm^{-2} with an ohmic resistance (R_{ohm}) of 0.061 Ω cm^2 and polarization resistance (R_p) of 0.044 Ω cm^2 at 650 °C (**Figure S20**). More outstanding electrochemical performances were demonstrated on the cell with the hybrid electrode, showing the peak power densities of 2.29, 1.72, 1.30, 0.94, and 0.64 W cm^{-2} at 650, 600, 550, 500, and 450 °C, respectively (**Figure 4B**). For reasonable comparisons, the R_{ohm} of the two cells kept identical, and the performance discrepancy may be mainly attributed to the decreasing R_p, such as a lower R_p of 0.038 Ω cm^2 for the hybrid electrode at 650 °C than PBC (**Figure 4C**). **Figure 4D** demonstrated the I-V curves of the electrolysis cell using wet air (3% H_2O) as the oxidant at 450-650 °C. The current densities of -3.12, -2.17, -1.36, -0.72, and -0.32 A cm^{-2} at 650-450 °C and 1.3 V were achieved for the cell with the hybrid electrode, higher than that (-2.57 A cm^{-2} at 650 °C and 1.3V) of the cell with the PBC electrode. The impressive peak power densities found with the hybrid electrode are better than most of the state-of-the-art air electrodes reported recently (**Table S7**),[3,5,21,26,44-53] such as $BaCo_{0.7}(Ce_{0.8}Y_{0.2})_{0.3}O_{3-\delta}$ (0.985 W cm^{-2} at 650 °C),[44] $PrBa_{0.5}Sr_{0.5}Co_{1.5}Fe_{0.5}O_{5+\delta}$ (1.40 W cm^{-2} at 650 °C)[47] and $PrNi_{0.5}Co_{0.5}O_{3-\delta}$ (1.7 W cm^{-2} at 600 °C in wet O_2)[5] (**Figure 4E** and **Figure S21**). The interface engineering can further improve electrochemical performance, exemplified by $BaSc_{0.1}Ta_{0.1}Co_{0.8}O_{3-\delta}$ perovskite air electrode via pulsed laser deposition (PLD) with a power density of 2.25 W cm^{-2} at 600 °C.[46] The obtained top electrolysis performance at 1.3 V and 600 °C (**Figure 4F** and **Table S8**) signifies that the hybrid electrode exhibits not only an enhanced activity of oxygen reduction reaction and excellent surface kinetics for oxygen evolution reaction.[5,6,22,26,27,45,49,51-55]

Figure 4G demonstrates the stability of a single cell in fuel-cell mode using H_2 as the fuel and air as the oxidant. For an extended duration of ~120 h under a current density of 0.5 A cm^{-2} at 550 °C, the cell showed no noticeable degradation, highlighting the great potential of robust air electrodes. Continuous degradation was found on the voltage of the cells with the PBC electrode at -0.5 A cm^{-2} and 550 °C under wet air (3% H_2O) within 38 h (**Figure 4H**). As judged by XRD and Raman spectra, the formation of impurities (likely $Ba(OH)_2$) may lead to the deactivation of the PBC air electrode and electrolysis performance degradation (**Figure S22**). When the PBC electrode was covered by the conformally high-entropy PNMCFC, the electrolysis stabilities under the applied current densities of -0.5 and -1 A cm^{-2} at 550 °C were largely improved for over 200 h, even in the hash humidified air (30% H_2O) (**Figure 4H**). Combined with the durable fuel-cell and electrolysis stability, a 2 h-fast reversible cycling was conducted at 550 °C and ±0.5 A cm^{-2}, exhibiting relatively stable with low degradation rates (**Figure 4I**). Faradaic efficiency is a critical standard for energy conversion from the H_2O to valuable H_2 production, theoretically defined as the ratio of the H_2 production rate detected by gas chromatography (GC) to that calculated by electron transfer number. When the applied current density was fixed at -1 A cm^{-2}, the Faradaic efficiencies were increased from 81.8% to 91.1%, with the steam concentration increasing from 3% to 60% (**Figure S23**). Such results were attributed to the high steam concentration, which can inhibit the electronic (electron-hole) conduction and provide more protons via hydration. Therefore, developing highly steam-tolerance air electrodes via high-entropy conformal coating can enhance the Faradaic efficiency for energy conversion and storage in the high-concentration steam electrolysis mode in a system of protonic ceramic cells.

Conclusion

In summary, the electrocatalytic activity and stability of the PBC electrode have been significantly enhanced by a wet-chemical solution infiltration of a high-entropy PNMCFC, which is more suitable for low-temperature PCCs. As steam is commonly encountered in PCCs, the impact of humidity on the electrocatalytic activity and structural stability of air electrodes is systemically investigated. Compared to the bare PBC electrode, the surface oxygen exchange kinetics of the hybrid electrode can be maintained without obvious deterioration by the high-entropy PNMCFC thin-film coating after interacting in wet air at 600 °C for 100 h. The surface composition examined by XPS and R_p stability directly indicated that the inherently robust interface between PBC and PNMCFC leads to performance and durability enhancements by suppressing water-mediated segregation. Due to faster oxygen exchange kinetics and unique architecture, the cell with the hybrid electrode obtained a higher power density of 1.30 W cm^{-2} and excellent stability for 120 h at 550 °C. Considering enhanced structural tolerance against steam, the hybrid electrode with conformal high entropy coating also exhibits outstanding advantages in the performance and stability of electrolysis modes and reversible cycling under a high-concentration humidified air (30% H_2O).

METHODS

The details of materials preparation, cell fabrication, materials characterization, and electrochemical measurements are provided in Supplemental Experimental Procedures.

RESOURCE AVAILABILITY

Lead contact

Further information and requests for information and resources should be directed to and will be fulfilled by the lead contact, Yu Chen (eschenyu@scut.edu.cn).

Materials availability

The new PNMCFC coating catalysts generated in this study will be made available on request.

Data and code availability

The data generated during this study are available in the main text and the supplemental information.

ACKNOWLEDGMENTS

This work was financially supported by the Introduced Innovative R&D Team of Guangdong (2021ZT09L392), the National Natural Science Foundation of China (22179039 and 22005105), the Fundamental Research Funds for the Central Universities (2022ZYGXZR002), the Pearl River Talent Recruitment Program (2019QN01C693), the Guangdong Basic and Applied Basic Research Foundation (2021A1515010395), and Zijin Mining Group Co., Ltd (5405-ZC-2023-00008). YMC acknowledges the National Science and Technology Council (NSTC Grant No. 111-2221-E-A49-003-MY3), the National Center for High-performance Computing (NCHC), and the Higher Education Sprout Project of the National Yang Ming Chiao Tung University and Ministry of Education (MOE), Taiwan. DFT calculations were performed using the resources of the Center for Functional Nanomaterials, which is a U.S. DOE Office of Science Facility, at Brookhaven National Laboratory under Contract No. DE-SC0012704.

AUTHOR CONTRIBUTIONS

Conceptualization, Y.C.; methodology, Y.C. and Y.L.; investigation, F.H., H.L., Y.X., K.S., and F.Z.; writing—original draft, F.H., Y.C., and Y.M.C.; writing—review & editing, Y.C., and Y.M.C.; funding acquisition, Y.L., Y.M.C., and Y.C.; resources, Y.M.C., and K.S.; supervision, Y.L., Y.M.C., and Y.C.

DECLARATION OF INTERESTS

The authors declare no competing interests.

SUPPLEMENTAL INFORMATION

Supplemental Information can be found online at.

REFERENCES

1. Ding, D., Li, X., Lai, S.Y., Gerdes, K., and Liu, M. (2014). Enhancing SOFC cathode performance by surface modification through infiltration. Energy & Environmental Science *7*, 552-575. https://doi.org/10.1039/C3EE42926A.
2. Zhan, Z., and Barnett, S.A. (2005). An octane-fueled solid oxide fuel cell. Science *308*, 844-847. https://doi.org/10.1126/science.1109213.
3. Duan, C., Tong, J., Shang, M., Nikodemski, S., Sanders, M., Ricote, S., Almansoori, A., and O'Hayre, R. (2015). Readily processed protonic ceramic fuel cells with high performance at low temperatures. Science *349*, 1321-1326. https://doi.org/10.1126/science.aab3987.
4. Li, X., Qin, H., Han, J., Jin, X., Xu, Y., Yang, S., Zhang, W., and Cao, R. (2024). A One - Pot Three - In - One Synthetic Strategy to Immobilize Cobalt Corroles on Carbon Nanotubes for Oxygen Electrocatalysis. Advanced Functional Materials *34*, 2310820. https://doi.org/10.1002/adfm.202310820.
5. Bian, W., Wu, W., Wang, B., Tang, W., Zhou, M., Jin, C., Ding, H., Fan, W., Dong, Y., and Li, J. (2022). Revitalizing interface in protonic ceramic cells by acid etch. Nature *604*, 479-485. https://doi.org/10.1038/s41586-022-04457-y.
6. Duan, C., Kee, R., Zhu, H., Sullivan, N., Zhu, L., Bian, L., Jennings, D., and O'Hayre, R. (2019). Highly efficient reversible protonic ceramic electrochemical cells for power generation and fuel production. Nature Energy *4*, 230-240. https://doi.org/10.1038/s41560-019-0333-2.
7. Duan, C., Kee, R.J., Zhu, H., Karakaya, C., Chen, Y., Ricote, S., Jarry, A., Crumlin, E.J., Hook, D., and Braun, R. (2018). Highly durable, coking and sulfur tolerant, fuel-flexible protonic ceramic fuel cells. Nature *557*, 217-222. https://doi.org/10.1038/s41586-018-0082-6.
8. Kim, J.H., Kim, D., Ahn, S., Kim, K.J., Jeon, S., Lim, D.-K., Kim, J.K., Kim, U., Im, H.-N., and Koo, B. (2023). An universal oxygen electrode for reversible solid oxide electrochemical cells at reduced temperatures. Energy & Environmental Science *16*, 3803-3814. https://doi.org/10.1039/D2EE04108A.
9. Zhao, Q., Zhang, Q., Xu, Y., Han, A., He, H., Zheng, H., Zhang, W., Lei, H., Apfel, U.-P., and Cao, R. (2024). Improving Active Site Local Proton Transfer in Porous Organic Polymers for Boosted Oxygen Electrocatalysis. Angewandte Chemie International Edition *63*, e202414104. https://doi.org/10.1002/anie.202414104.
10. Wachsman, E.D., and Lee, K.T. (2011). Lowering the temperature of solid oxide fuel cells. Science *334*, 935-939. https://doi.org/10.1126/science.1204090.
11. Duan, C., Huang, J., Sullivan, N., and O'Hayre, R. (2020). Proton-conducting oxides for energy conversion and storage. Applied Physics Reviews *7*, 011314. https://doi.org/10.1063/1.5135319.
12. Steele, B.C., and Heinzel, A. (2001). Materials for fuel-cell technologies. Nature *414*, 345-352. https://doi.org/10.1038/35104620.
13. Zhu, F., Hou, M., Du, Z., He, F., Xu, Y., Xu, K., Gao, H., Liu, Y., and Chen, Y. (2024). Steam-promoted symmetry optimizations of perovskite electrodes for protonic ceramic cells. Energy & Environmental Science *17*, 7782-7791. https://doi.org/10.1039/D4EE02233E.
14. Liu, Z., Bai, Y., Sun, H., Guan, D., Li, W., Huang, W.-H., Pao, C.-W., Hu, Z., Yang, G., and Zhu, Y. (2024). Synergistic dual-phase air electrode enables high and durable performance of reversible proton ceramic electrochemical cells. Nature Communications *15*, 472. https://doi.org/10.1038/s41467-024-44767-5.
15. Luo, Z., Zhou, Y., Hu, X., Kane, N., Li, T., Zhang, W., Liu, Z., Ding, Y., Liu, Y., and Liu, M. (2022). Critical role of acceptor dopants in designing highly stable and compatible proton-conducting electrolytes for reversible solid oxide cells. Energy & Environmental Science *15*, 2992-3003.

https://doi.org/10.1039/D2EE01104B.

16. Kim, J.H., Yoo, S., Murphy, R., Chen, Y., Ding, Y., Pei, K., Zhao, B., Kim, G., Choi, Y., and Liu, M. (2021). Promotion of oxygen reduction reaction on a double perovskite electrode by a water-induced surface modification. Energy & Environmental Science *14*, 1506-1516. https://doi.org/10.1039/D0EE03283B.

17. Pei, K., Zhou, Y., Xu, K., Zhang, H., Ding, Y., Zhao, B., Yuan, W., Sasaki, K., Choi, Y., and Chen, Y. (2022). Surface restructuring of a perovskite-type air electrode for reversible protonic ceramic electrochemical cells. Nature communications *13*, 2207. https://doi.org/10.1038/s41467-022-29866-5.

18. Xu, K., Zhang, H., Xu, Y., He, F., Zhou, Y., Pan, Y., Ma, J., Zhao, B., Yuan, W., and Chen, Y. (2022). An efficient steam-induced heterostructured air electrode for protonic ceramic electrochemical cells. Advanced Functional Materials, 2110998. https://doi.org/10.1002/adfm.202110998.

19. Zhou, Y., Zhang, W., Kane, N., Luo, Z., Pei, K., Sasaki, K., Choi, Y., Chen, Y., Ding, D., and Liu, M. (2021). An efficient bifunctional air electrode for reversible protonic ceramic electrochemical cells. Advanced Functional Materials *31*, 2105386. https://doi.org/10.1002/adfm.202105386.

20. Shao, Z.P., and Haile, S.M. (2004). A high-performance cathode for the next generation of solid-oxide fuel cells. Nature *431*, 170-173. https://doi.org/10.1038/nature02863.

21. Gao, H., He, F., Zhu, F., Xia, J., Du, Z., Huang, Y., Zhu, L., and Chen, Y. (2024). Effective promotion of the activity and stability of cathodes for protonic ceramic fuel cells. Advanced Functional Materials, 2401747. https://doi.org/10.1002/adfm.202401747.

22. He, F., Zhou, Y., Hu, T., Xu, Y., Hou, M., Zhu, F., Liu, D., Zhang, H., Xu, K., and Liu, M. (2023). An efficient high-entropy perovskite-type air electrode for reversible oxygen reduction and water splitting in protonic ceramic cells. Advanced Materials, 2209469. https://doi.org/10.1002/adma.202209469.

23. Koo, B., Kim, K., Kim, J.K., Kwon, H., Han, J.W., and Jung, W. (2018). Sr segregation in perovskite oxides: why it happens and how it exists. Joule *2*, 1476-1499. https://doi.org/10.1016/j.joule.2018.07.016

24. Lee, W., Han, J.W., Chen, Y., Cai, Z., and Yildiz, B. (2013). Cation size mismatch and charge interactions drive dopant segregation at the surfaces of manganite perovskites. Journal of the American Chemical Society *135*, 7909-7925. https://doi.org/10.1021/ja3125349.

25. Zhou, X.-D., Templeton, J.W., Nie, Z., Chen, H., Stevenson, J.W., and Pederson, L.R. (2012). Electrochemical performance and stability of the cathode for solid oxide fuel cells: V. high performance and stable Pr_2NiO_4 as the cathode for solid oxide fuel cells. Electrochimica Acta *71*, 44-49. https://doi.org/10.1016/j.electacta.2012.03.067.

26. Saqib, M., Choi, I.-G., Bae, H., Park, K., Shin, J.-S., Kim, Y.-D., Lee, J.-I., Jo, M., Kim, Y.-C., and Lee, K.-S. (2021). Transition from perovskite to misfit-layered structure materials: a highly oxygen deficient and stable oxygen electrode catalyst. Energy & Environmental Science *14*, 2472-2484. https://doi.org/10.1039/D0EE02799E.

27. Liu, Z., Tang, Z., Song, Y., Yang, G., Qian, W., Yang, M., Zhu, Y., Ran, R., Wang, W., and Zhou, W. (2022). High-entropy perovskite oxide: A new opportunity for developing highly active and durable air electrode for reversible protonic ceramic electrochemical cells. Nano-Micro Letters *14*, 217. https://doi.org/10.1007/s40820-022-00967-6.

28. Han, X., Ling, Y., Yang, Y., Wu, Y., Gao, Y., Wei, B., and Lv, Z. (2023). Utilizing high entropy effects for developing chromium-tolerance cobalt-free cathode for solid oxide fuel cells. Advanced Functional Materials *33*, 2304728. https://doi.org/10.1002/adfm.202304728.

29. Sarkar, A., Velasco, L., Wang, D., Wang, Q., Talasila, G., de Biasi, L., Kübel, C., Brezesinski, T., Bhattacharya, S.S., Hahn, H., and Breitung, B. (2018). High entropy oxides for reversible energy storage. Nature Communications *9*, 3400. https://doi.org/10.1038/s41467-018-05774-5.

30. Salman, M., Saleem, S., Ling, Y., and Khan, M. (2024). Fe-based high-entropy perovskite oxide: A strategy to suppress Sr segregation and performance evaluation as an electrode material for SOFCs. ACS Applied Energy Materials *7*, 8648-8657. https://doi.org/10.1021/acsaem.4c01614.

31. Hu, T., He, F., Liu, M., and Chen, Y. (2023). In situ/operando regulation of the reaction activities on hetero-structured electrodes for solid oxide cells. Progress in Materials Science *133*, 101050. https://doi.org/10.1016/j.pmatsci.2022.101050.

32. Shchukin, D.G., and Caruso, R.A. (2004). Template synthesis and photocatalytic properties of porous metal oxide spheres formed by nanoparticle infiltration. Chemistry of Materials *16*, 2287-2292. https://doi.org/10.1021/cm0497780.

33. Fang, W., Steinbach, F., Cao, Z., Zhu, X., and Feldhoff, A. (2016). A highly efficient sandwich‐like symmetrical dual‐phase oxygen‐transporting membrane reactor for hydrogen production by water splitting. Angewandte Chemie International Edition *55*, 8648-8651. https://doi.org/10.1002/anie.201603528.

34. Tsvetkov, N., Lu, Q., Sun, L., Crumlin, E.J., and Yildiz, B. (2016). Improved chemical and electrochemical stability of perovskite oxides with less reducible cations at the surface. Nature materials *15*, 1010-1016. https://doi.org/10.1038/nmat4659.

35. Lynch, M.E., Yang, L., Qin, W., Choi, J.-J., Liu, M., Blinn, K., and Liu, M. (2011). Enhancement of $La_{0.6}Sr_{0.4}Co_{0.2}Fe_{0.8}O_{3-\delta}$ durability and surface electrocatalytic activity by $La_{0.85}Sr_{0.15}MnO_{3\pm\delta}$ investigated using a new test electrode platform. Energy & Environmental Science *4*, 2249-2258. https://doi.org/10.1039/c1ee01188j.

36. Akrami, S., Edalati, P., Fuji, M., and Edalati, K. (2021). High-entropy ceramics: Review of principles, production and applications. Materials Science and Engineering: R: Reports *146*, 100644. https://doi.org/10.1016/j.mser.2021.100644.

37. He, F., Zhu, F., Liu, D., Zhou, Y., Sasaki, K., Choi, Y., Liu, M., and Chen, Y. (2023). A reversible perovskite air electrode for active and durable oxygen reduction and evolution reactions via the A-site entropy engineering. Materials Today *63*, 89-98. https://doi.org/10.1016/j.mattod.2023.02.006.

38. Chen, Y., Yoo, S., Choi, Y., Kim, J.H., Ding, Y., Pei, K., Murphy, R., Zhang, Y., Zhao, B., and Zhang, W. (2018). A highly active, CO_2-tolerant electrode for the oxygen reduction reaction. Energy & Environmental Science *11*, 2458-2466. https://doi.org/10.1039/C8EE01140K.

39. Shen, L., Du, Z., Zhang, Y., Dong, X., and Zhao, H. (2021). Medium-entropy perovskites $Sr(Fe_{\alpha}Ti_{\beta}Co_{\gamma}Mn_{\zeta})O_{3-\delta}$ as promising cathodes for intermediate temperature solid oxide fuel cell. Applied Catalysis B: Environmental *295*, 120264. https://doi.org/10.1016/j.apcatb.2021.120264.

40. Choi, S.M., An, H., Yoon, K.J., Kim, B.-K., Lee, H.-W., Son, J.-W., Kim, H., Shin, D., Ji, H.-I., and Lee, J.-H. (2019). Electrochemical analysis of high-performance protonic ceramic fuel cells based on a columnar-structured thin electrolyte. Applied Energy *233*, 29-36. https://doi.org/10.1016/j.apenergy.2018.10.043.

41. Zhai, S., Xie, H., Cui, P., Guan, D., Wang, J., Zhao, S., Chen, B., Song, Y., Shao, Z., and Ni, M. (2022). A combined ionic Lewis acid descriptor and machine-learning approach to prediction of efficient oxygen reduction electrodes for ceramic fuel cells. Nature Energy *7*, 866-875. https://doi.org/10.1038/s41560-022-01098-3.

42. He, F., Wu, T., Peng, R., and Xia, C. (2009). Cathode reaction models and performance analysis of $Sm_{0.5}Sr_{0.5}CoO_{3-\delta}$–$BaCe_{0.8}Sm_{0.2}O_{3-\delta}$ composite cathode for solid oxide fuel cells with proton conducting electrolyte. Journal of Power Sources *194*, 263-268. https://doi.org/10.1016/j.jpowsour.2009.04.053.

43. Wang, H., Zhai, T., Wu, Y., Zhou, T., Zhou, B., Shang, C., and Guo, Z. (2023). High-Valence Oxides for High Performance Oxygen Evolution Electrocatalysis. Advanced Science *10*, 2301706. https://doi.org/10.1002/advs.202301706.

44. Song, Y., Chen, Y., Wang, W., Zhou, C., Zhong, Y., Yang, G., Zhou, W., Liu, M., and Shao, Z. (2019). Self-assembled triple-conducting nanocomposite as a superior protonic ceramic fuel cell cathode. Joule *3*, 2842-2853. https://doi.org/10.1016/j.joule.2019.07.004

45. Pei, K., Luo, S., He, F., Arbiol, J., Xu, Y., Zhu, F., Wang, Y., and Chen, Y. (2023). Constructing an active and stable oxygen electrode surface for reversible protonic ceramic electrochemical cells. Applied Catalysis B: Environmental *330*, 122601. https://doi.org/10.1016/j.apcatb.2023.122601.

46. Kim, D., Jeong, I., Ahn, S., Oh, S., Im, H.N., Bae, H., Song, S.J., Lee, C.W., Jung, W., and Lee, K.T. (2024). On the Role of Bimetal‐Doped $BaCoO_{3-\delta}$ Perovskites as

Highly Active Oxygen Electrodes of Protonic Ceramic Electrochemical Cells. Advanced Energy Materials *14*, 2304059. https://doi.org/10.1002/aenm.202304059.

47. Choi, S., Kucharczyk, C.J., Liang, Y., Zhang, X., Takeuchi, I., Ji, H.-I., and Haile, S.M. (2018). Exceptional power density and stability at intermediate temperatures in protonic ceramic fuel cells. Nature Energy *3*, 202-210. https://doi.org/10.1038/s41560-017-0085-9.

48. Liu, F., Deng, H., Diercks, D., Kumar, P., Jabbar, M.H.A., Gumeci, C., Furuya, Y., Dale, N., Oku, T., and Usuda, M. (2023). Lowering the operating temperature of protonic ceramic electrochemical cells to <450° C. Nature Energy *8*, 1145-1157. https://doi.org/10.1038/s41560-023-01350-4.

49. He, F., Hou, M., Liu, D., Ding, Y., Sasaki, K., Choi, Y., Guo, S., Han, D., Liu, Y., and Liu, M. (2024). Phase segregation of a composite air electrode unlocks the high performance of reversible protonic ceramic electrochemical cells. Energy & Environmental Science *17*, 3898-3907. https://doi.org/10.1039/D4EE01608D.

50. Kim, J.H., Hong, J., Lim, D.K., Ahn, S., Kim, J., Kim, J.K., Oh, D., Jeon, S., Song, S.J., and Jung, W. (2022). Water as a hole-predatory instrument to create metal nanoparticles on triple-conducting oxides. Energy & Environmental Science *15*, 1097-1105. https://doi.org/10.1039/d1ee03046a.

51. Ding, H., Wu, W., Jiang, C., Ding, Y., Bian, W., Hu, B., Singh, P., Orme, C.J., Wang, L., and Zhang, Y. (2020). Self-sustainable protonic ceramic electrochemical cells using a triple conducting electrode for hydrogen and power production. Nature communications *11*, 1907. https://doi.org/10.1038/s41467-020-15677-z.

52. Chen, X., Yu, N., Song, Y., Liu, T., Xu, H., Guan, D., Li, Z., Huang, W.H., Shao, Z., and Ciucci, F. (2024). Synergistic bulk and surface engineering for expeditious and durable reversible protonic ceramic electrochemical cells air electrode. Advanced Materials, 2403998. https://doi.org/10.1002/adma.202403998.

53. Park, K., Saqib, M., Lee, H., Shin, D., Jo, M., Park, K.M., Hamayun, M., Kim, S.H., Kim, S., and Lee, K.-S. (2024). Water-mediated exsolution of nanoparticles in alkali metal-doped perovskite structured triple-conducting oxygen electrocatalysts for reversible cells. Energy & Environmental Science *17*, 1175-1188. https://doi.org/10.1039/D3EE03510G.

54. Kim, J., Jun, A., Gwon, O., Yoo, S., Liu, M., Shin, J., Lim, T.-H., and Kim, G. (2018). Hybrid-solid oxide electrolysis cell: A new strategy for efficient hydrogen production. Nano Energy *44*, 121-126. https://doi.org/10.1016/j.nanoen.2017.11.074.

55. Choi, S., Davenport, T.C., and Haile, S.M. (2019). Protonic ceramic electrochemical cells for hydrogen production and electricity generation: exceptional reversibility, stability, and demonstrated faradaic efficiency. Energy & Environmental Science *12*, 206-215. https://doi.org/10.1039/C8EE02865F